materials

MDPI

Article

Synthesis, Structural Property, Photophysical Property, Photocatalytic Property of Novel $ZnBiErO_4$ under Visible Light Irradiation

Jingfei Luan [1,2,*] and Yan Zhuang [2]

[1] School of Chemistry and Environmental Engineering, Changchun University of Science and Technology, Changchun 130600, China

[2] State Key Laboratory of Pollution Control and Resource Reuse, School of the Environment, Nanjing University, Nanjing 210093, China; yanzhuang1011@yahoo.com

* Correspondence: jfluan@nju.edu.cn; Tel.: +86-13585206718; Fax: +86-25-89680397

Received: 29 December 2017; Accepted: 30 January 2018; Published: 18 February 2018

Abstract: A novel photocatalyst $ZnBiErO_4$ was firstly synthesized by solid-state reaction method and its structural and photocatalytic properties were analyzed by scanning electron microscopy, X-ray diffraction, X-ray photoelectron spectroscopy and UV-Vis diffuse reflectance. The results demonstrated that $ZnBiErO_4$ crystallized with tetragonal crystal structure with space group I41/A. The lattice parameters for $ZnBiErO_4$ were proved to be a = b = 10.255738 Å and c = 9.938888 Å. The band gap of $ZnBiErO_4$ was estimated to be about 1.69 eV. Compared with nitrogen doped TiO_2, $ZnBiErO_4$ showed excellent photocatalytic activities for degrading methyl blue during visible light irradiation. The photocatalytic degradation of methyl blue with $ZnBiErO_4$ or N-doped TiO_2 as catalyst followed the first-order reaction kinetics. Moreover, the apparent first-order rate constant of $ZnBiErO_4$ or N-doped TiO_2 was 0.01607 min^{-1} or 0.00435 min^{-1}. The reduction of total organic carbon, formation of inorganic products, such as SO_4^{2-} and NO_3^- and the evolution of CO_2 revealed the continuous mineralization of methyl blue during the photocatalytic process. $ZnBiErO_4$ photocatalyst had great potential to purify textile industry wastewater.

Keywords: $ZnBiErO_4$; photocatalyst; methyl blue; photocatalytic degradation; visible light irradiation

1. Introduction

The organic pollutants of dye wastewater formatted by the industrial production, are toxicity, unacceptable color, high chemical oxygen demand and biological degradation, which caused the difficulty of self-degradation in natural conditions [1]. It will not only get undesirable result but also produce benzene, aniline and other secondary pollutants sometimes when we degrade it by traditional treatment methods [2–7]. In recent years, photocatalysis has caused general concern because of its strong oxidizability to degrade many organic pollutants in wastewater and effluents, especially for the dyes wastewater [8–15]. In recent years, as a semiconductor, TiO_2 photocatalyst has attracted wide attention owing to the property of non-toxic, excellent stability and low cost [16–18]. However, due to the wide band gap (3.2 eV) of TiO_2, the required wavelength is less than 387.5 nm, which near ultraviolet light and occupies only 4~5% of the solar energy and thus limits its application [19,20]. Although a variety of methods have been tried to modify TiO_2, its quantum efficiency is still very low and the modification brings more shortcomings [21–26]. Based on the reason, it is necessary to develop new visible light responsive photocatalysts to utilize more visible light, which accounts for about 43% of the solar energy. Therefore, it is of grate important to develop the catalysts which can response to visible light. And many scientists have engaged in photocatalysis using visible light today [27–35].

AB_2O_4-type spinel composite oxides with narrow band gap have attracted extensive attention because of its excellent visible light response in textile wastewater treatment in recent years. They are capable to be used in adsorption, photocatalysis, hydrogen production and chemical sensors. It is demonstrated that $NiCo_2O_4$ and $ZnFe_2O_4$ exhibited a good photocatalytic activity for degrading methylene blue and other organic under visible light irradiation [36,37]. $CoAl_2O_4$ films were prepared in different structure, composition, morphology and optical properties by the method of chemical vapor deposition in 800–1200 °C by Carta et al. and its high photocatalytic activity were demonstrated [38]. The spinel oxide $CaBi_2O_4$ synthesized by Tang et al. could not only degrade gas phase acetaldehyde and MB aqueous solution under visible light irradiation but also keep high catalyst recovery [39]. $ZnCo_2O_4$ nanoparticles were synthesized by a co-precipitation decomposition method and the optical band gap of the nanoparticles was estimated to be 3.39 eV from the UV-Vis absorption spectrum. On the basis of the laboratory test results, the $ZnCo_2O_4$ nanoparticles performed a high photocatalytic activity for the degradation of methyl blue dye solution under visible light irradiation [40]. $ZnBiGaO_4$ was prepared to photocatalytic decompose hydrogen sulfide (H_2S) with two different methods under visible light irradiation, its band gap was estimated to be 2.8 eV [41]. $MgFe_2O_4$/PANI photocatalyst, which was synthesized by hydrothermal synthesis method, proved a high effective photodecolorization of both methylene blue and methyl orange dyes in aqueous solution and maintained a high removal ability after five repeated utilizations [42].

$ZnBiErO_4$ is a material that has never been synthesized and the data about its structural and photocatalytic properties such as space group and lattice constants have not been found before. $ZnBiErO_4$ seems to have a potential to improve the photocatalytic activity, because it has been proved that a slight modification of a semiconductor structure will result in a remarkable change in photocatalytic properties [43]. Herein, $ZnBiErO_4$ was prepared by the solid-state reaction method for the first time. We studied its structure and photocatalytic properties through a series of characterizations. Photocatalytic performances of $ZnBiErO_4$ in the degradation of methyl blue (MB) under visible light were also investigated. At the same time, we made a comparison between $ZnBiErO_4$ and N-doped titanium dioxide to discover their differences in photocatalytic activity. The experimental results showed that the catalytic system with $ZnBiErO_4$ revealed unusual catalytic effects for MB under visible light irradiation.

2. Results and Discussion

2.1. Characterization

Figure 1 is the scanning electron microscope-X-ray energy dispersion (SEM-EDS) spectrum of the as-synthesized $ZnBiErO_4$. The composition was analyzed by EDS and the result was in line with that of XRD patterns. According to the SEM-EDS spectrum, the prepared $ZnBiErO_4$ was composed of the elements of zinc, bismuth, Erbium and oxygen, furthermore, the mean atomic ratio of Zn:Bi:Er:O was estimated to be 1:1:1:4. Fortunately, other elements were not traced, which showed that our prepared $ZnBiErO_4$ catalyst was pure phase without any other impurities. The SEM image shows the morphology of $ZnBiErO_4$ particle and the irregular shape and uniform particle size of $ZnBiErO_4$ were observed. Figure 2 shows a typical transmission electron microscopy (TEM) image of $ZnBiErO_4$ catalyst, which reveals that the average particle diameter of $ZnBiErO_4$ was about 350 nm. The corresponding selected-area electron diffraction (SAED) pattern is presented in Figure 3, showing discrete diffraction rings. It is suggested that the single sheet was comprised by multi crystals. Figure 4 is the diagram of particle size of $ZnBiErO_4$ catalyst, which indicated that the particle size of $ZnBiErO_4$ was mainly distributed in 326~387 nm. The result was in line with the TEM.

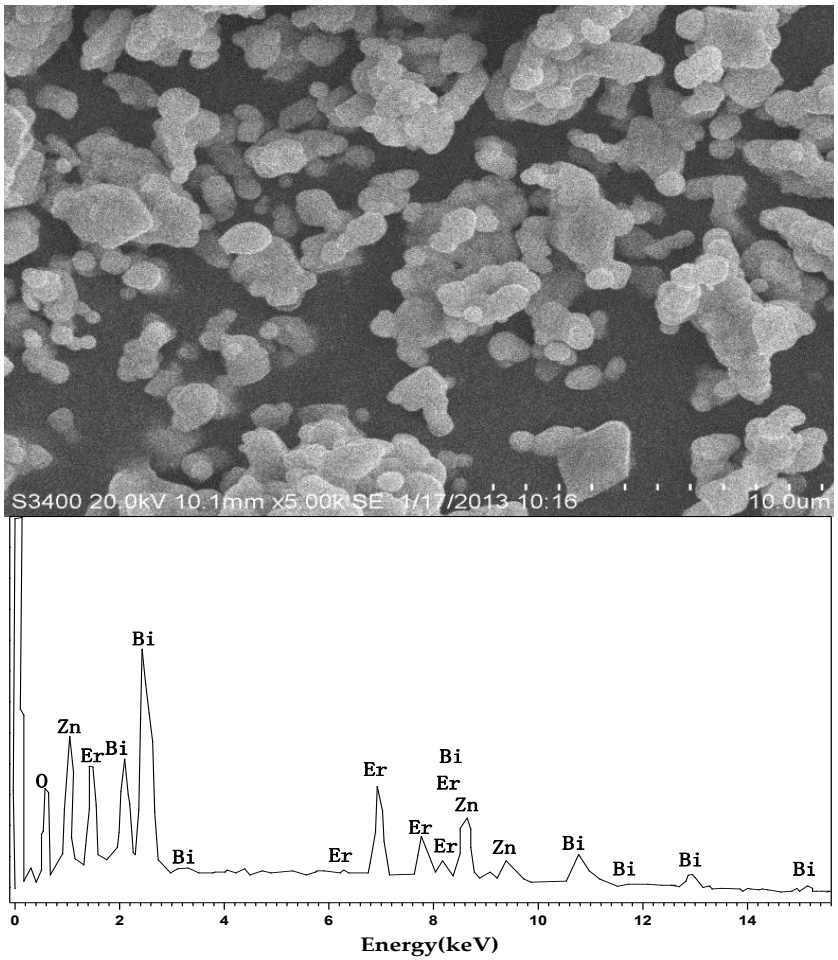

Figure 1. SEM-EDS spectrum of $ZnBiErO_4$.

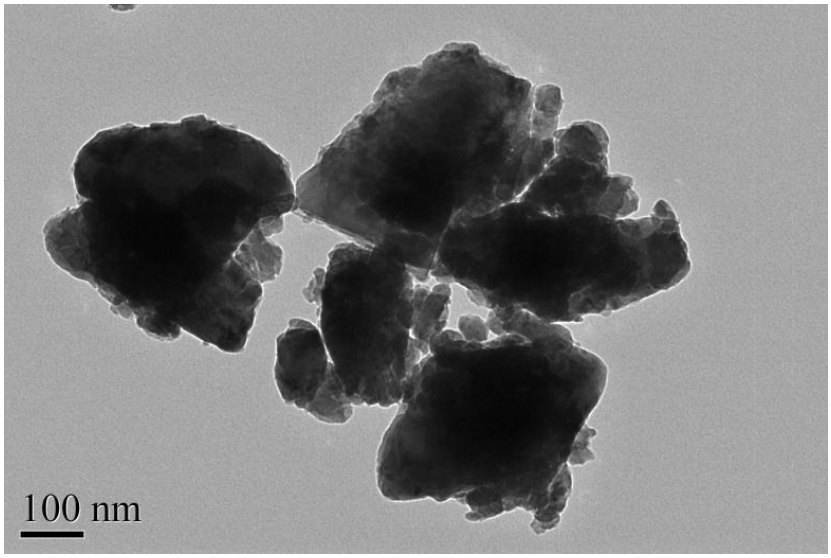

Figure 2. TEM image of $ZnBiErO_4$.

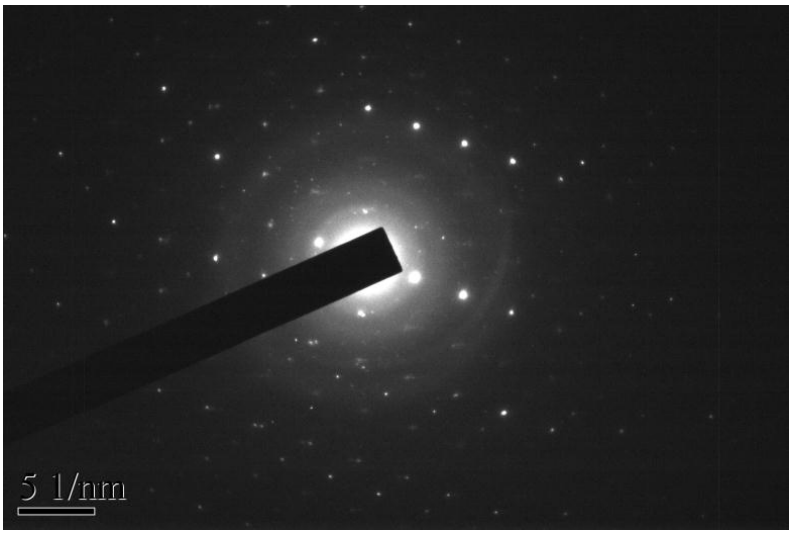

Figure 3. The selected area electron diffraction pattern of $ZnBiErO_4$.

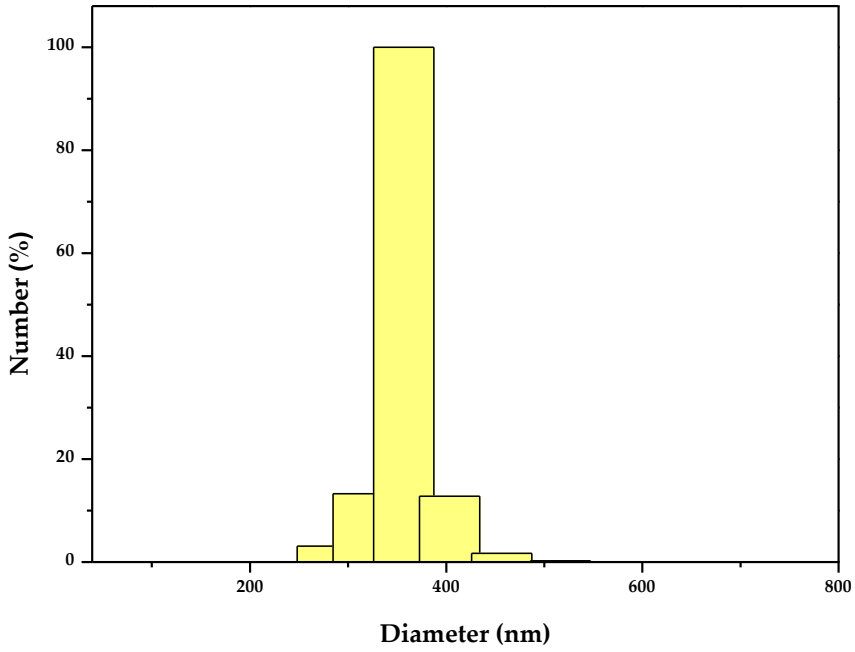

Figure 4. The diagram of particle size of $ZnBiErO_4$.

Figure 5 represents the X-ray powder diffraction patterns of $ZnBiErO_4$, ZnO, Bi_2O_3 and Er_2O_3. Compared to the individual oxides used in synthesis, the synthesized photocatalyst was proved to be novel and it was not the mixture of individual oxides sintered at high temperature. Full-profile structure refinements of the collected X-ray diffraction data of $ZnBiErO_4$ were continued to investigate by the RIETAN^{TM} program, which was based on Pawley analysis. The obtained XRD patterns of $ZnBiErO_4$ samples are shown in Figure 6. It is demonstrated that the observed intensities were in according with the calculated intensities in a tetragonal crystal structure with space group I41/A. The lattice parameters for $ZnBiErO_4$ were proved to be a = b = 10.255738 Å and c = 9.938888 Å. According to the lattice constants and the space group I41/A. All of the diffraction peaks for $ZnBiErO_4$ could be successfully indexed and no other impurity phases are found, showing the single phase of the products. The result was in line with SEM-EDS spectrum. In order to simulate the structure of $ZnBiErO_4$ accurately, Pawley refinements of the XRD spectrum and the three-dimensional space

structure model of $ZnBiErO_4$ photocatalyst were established by Material Studio software (Material Studio 2.0, Accelrys Corporation, USA). The atomic coordinates and structural parameters of $ZnBiErO_4$ are listed in Table 1 and the atomic structure of $ZnBiErO_4$ is shown in Figure 7.

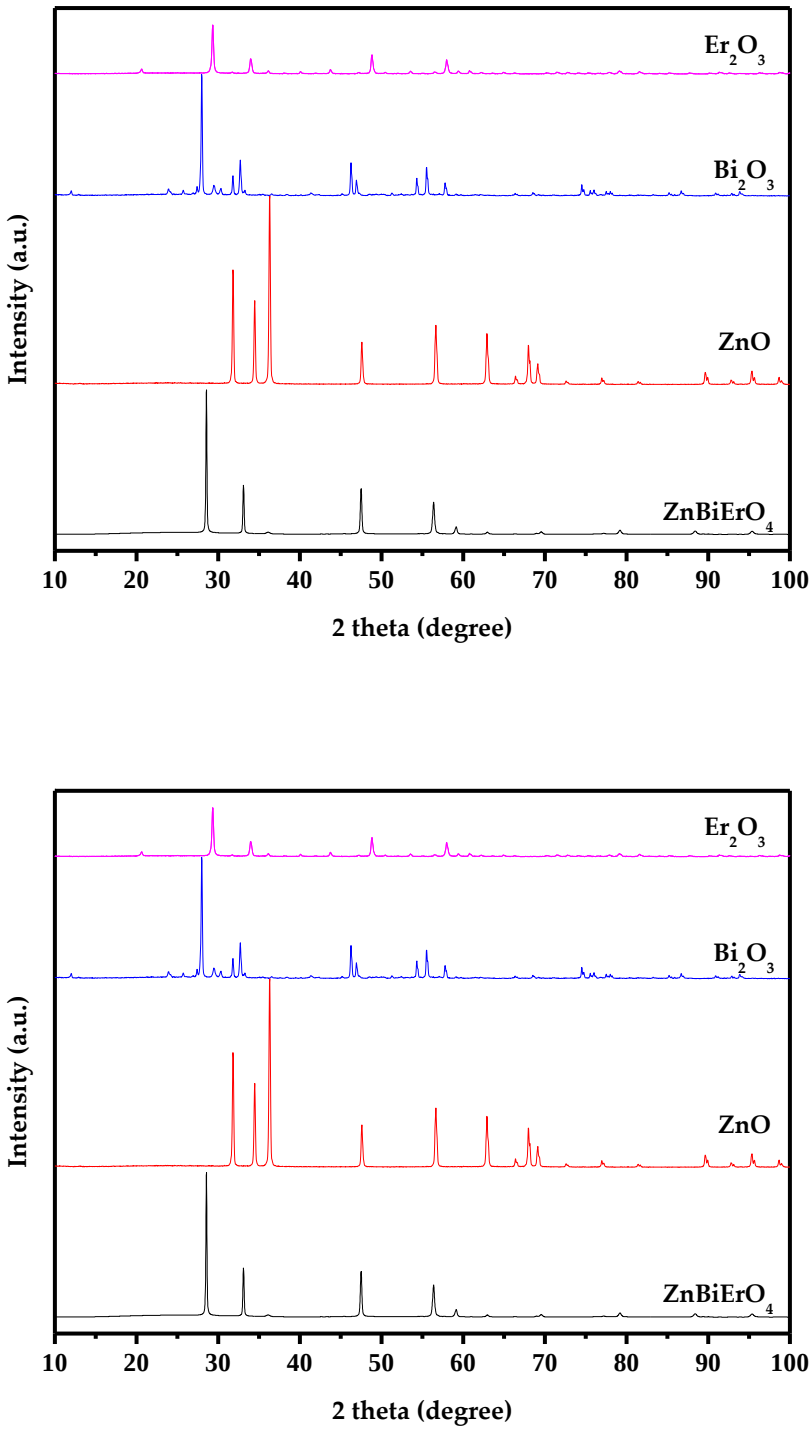

Figure 5. X-ray powder diffraction patterns of $ZnBiErO_4$, ZnO, Bi_2O_3 and Er_2O_3.

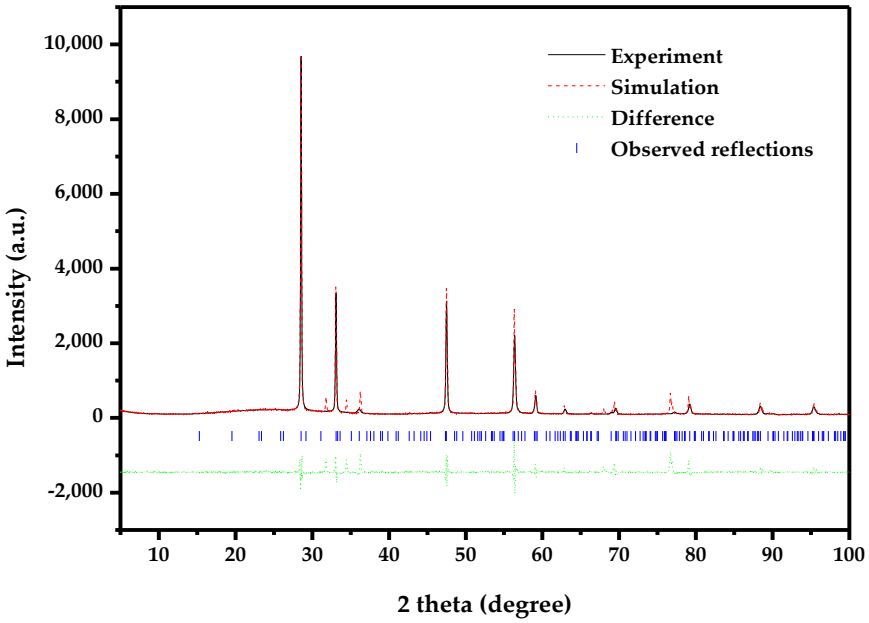

Figure 6. Pawley refinements of XRD data for novel photocatalyst $ZnBiErO_4$ prepared by the solid-state reaction method at 1000 °C. The solid line represents experimental X-ray diffraction pattern. The dot line represents simulation X-ray diffraction pattern. The tic marks represent reflection position. A difference between observed and calculated profile is shown beneath.

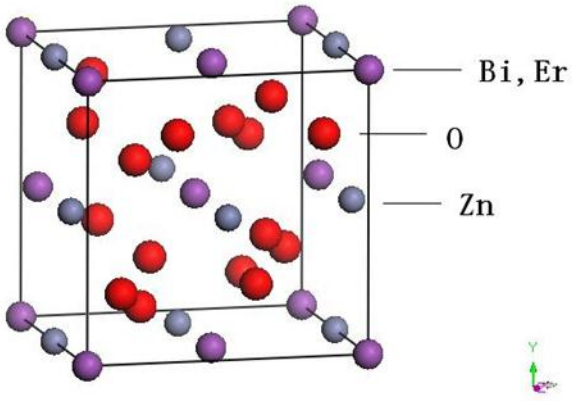

Figure 7. Atomic structure of $ZnBiErO_4$.

Table 1. Atomic coordinates and structural parameters of $ZnBiErO_4$ prepared by the solid reaction method.

Atom	x	y	z	Occupation Factor
Zn	0	0	0.5	1
Bi	0	0	0	1
Er	0	0	0	1
O	0.76731	0.14013	0.08188	1

In order to get the surface chemical compositions and the valence states of various elements of $ZnBiErO_4$, the X-ray photoelectron spectrum (XPS) was carried out. The XPS full spectrum and detailed spectrum of $ZnBiErO_4$ are shown in Figure 8. To see the results clearly, various elemental peaks with specific binding energies are provided in Table 2. According to the XPS full spectrum in

Figure 8a, the synthesized $ZnBiErO_4$ contained the elements of Zn, Bi, Er, O and C. The element of C was come from hydrocarbon for the sake of testing, so it was in agreement with the results of SEM-EDS. By fitting and separating the peak, we got the XPS detailed spectrum in Figure 8b–e. $Zn2p_{1/2}$ and $Zn2p_{3/2}$ peaks of Zn element were seen in Figure 8b, whose positions were 1043.6 eV and 1023.3 eV, respectively. $Bi4f_{7/2}$ and $Bi4f_{5/2}$ peaks of Bi element were observed in Figure 8c, whose positions were 157.7 eV and 163.0 eV, respectively. And the Er4d peak of Er element was presented in Figure 8d, whose position was 162.9 eV. It was obvious to find that there existed shoulders peaks at the XPS spectrum of O1s. By fitting and separating the peak, we got $O_{Lattice}$ peak and $O_{Absorbed}$ peak, which indicated that the catalyst absorbed some O_2 in the process of calcination. Otherwise, the results showed that the oxidation states of Zn, Bi, Er and O ions from $ZnBiErO_4$ were +2, +3, +3 and −2, respectively. Therefore, it could be deduced that the resulting material was highly pure under our preparation conditions. Notably, neither shoulders nor widening in the XPS peaks of $ZnBiErO_4$ was observed, indicating the absence of any other phases.

Table 2. Binding energies (BE) for key elements from $ZnBiErO_4$.

Compound	$Zn2p_{1/2}$ BE (eV)	$Zn2p_{3/2}$ BE (eV)	$Bi4f_{7/2}$ BE (eV)	$Bi4f_{5/2}$ BE (eV)	Er4d BE (eV)	O1s BE (eV)
$ZnBiErO_4$	1043.6	1020.3	157.7	163.0	162.9	529.8

The UV-vis absorption spectra of $ZnBiErO_4$ and N-doped TiO_2 are shown in Figure 9. In contrast to the N-doped TiO_2, whose absorption edge was 414 nm, the novel synthesized $ZnBiErO_4$ photocatalyst exhibited an obvious absorption in the visible region up to 690 nm. Furthermore, the band gap of $ZnBiErO_4$ and N-doped TiO_2 by extrapolating the linear portion of the curve to zero absorbance are 1.69 eV and 2.76 eV, respectively. It indicated that $ZnBiErO_4$ could be excited by visible light and might exhibit a better visible light photocatalytic activity. Apparently, reflection and scattering did not cause a significant absorption.

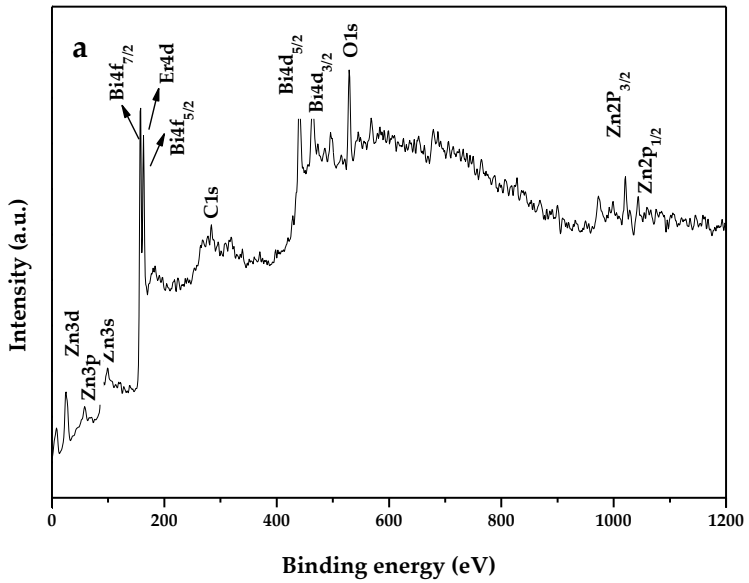

Figure 8. *Cont.*

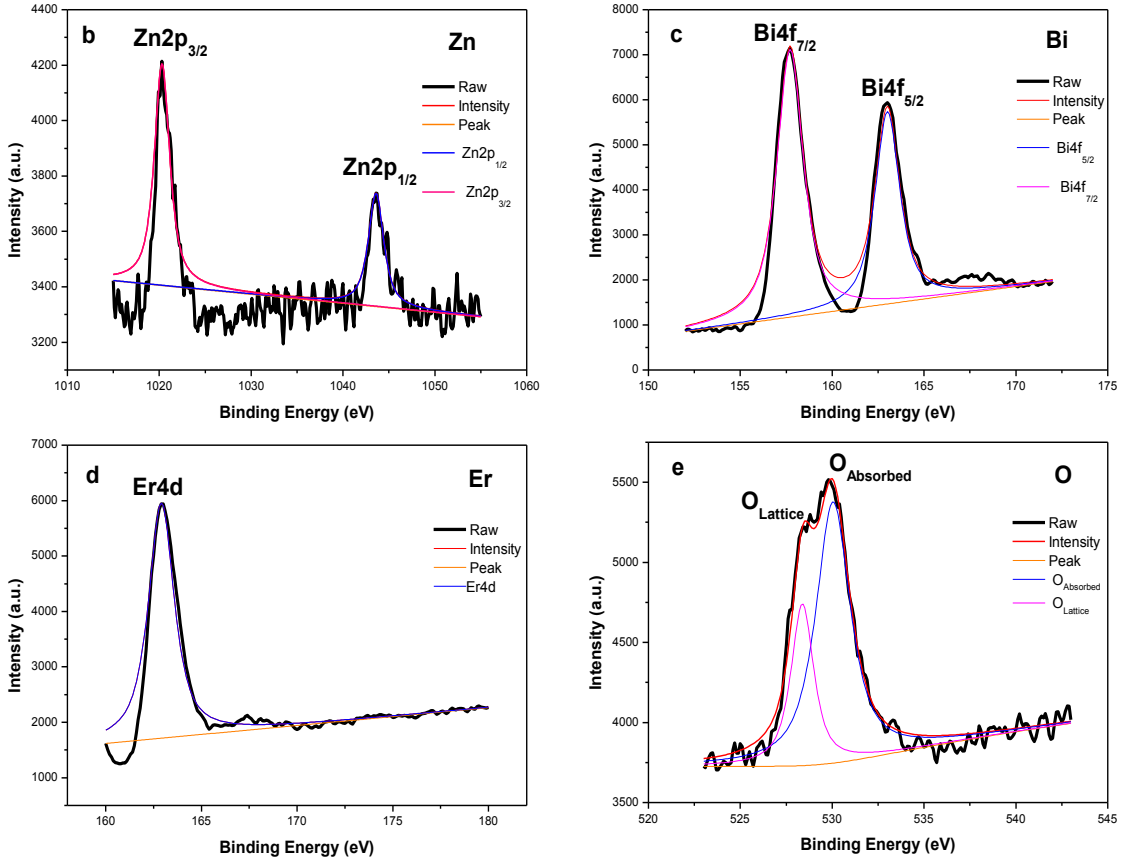

Figure 8. (**a**) The XPS full spectrum of $ZnBiErO_4$; (**b**) Zn2p spectrum of $ZnBiErO_4$; (**c**) Bi4f spectrum of $ZnBiErO_4$; (**d**) Er4d spectrum of $ZnBiErO_4$; (**e**) O1s spectrum of $ZnBiErO_4$.

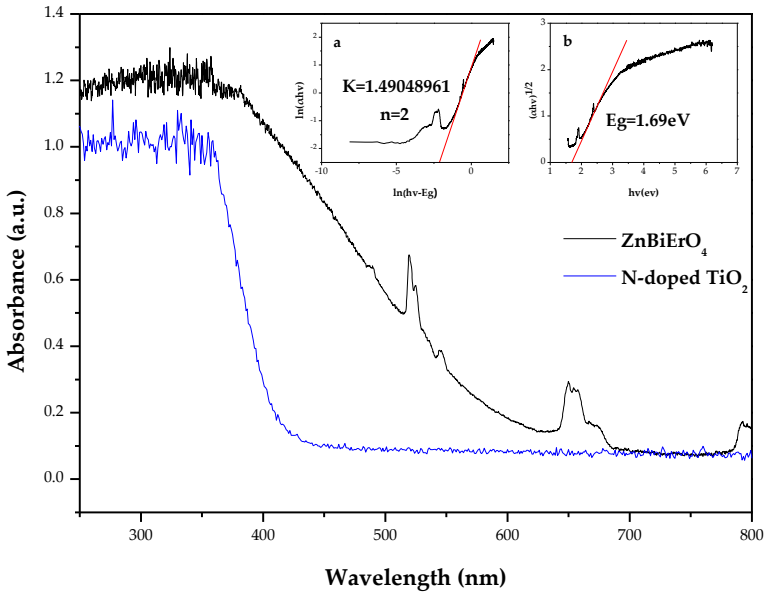

Figure 9. UV-Vis absorption spectra of $ZnBiErO_4$ and N-doped TiO_2. (**a**) plot of $\ln(\alpha h\nu)$ versus $\ln(h\nu - E_g)$ for $ZnBiErO_4$. (**b**) plot of $(\alpha h\nu)^{1/2}$ versus $h\nu$ for $ZnBiErO_4$.

For a crystalline semiconductor, the optical absorption near the band edge followed the equation [44]:

$$\alpha h\nu = \mathrm{A}(h\nu - E_g)^n \quad (1)$$

Here, A, α, E_g and ν are proportional constant, absorption coefficient, band gap and light frequency, respectively. Within this equation, n determines the character of the transition in a semiconductor. E_g and n can be calculated by the following steps: (i) plotting $\ln(\alpha h\nu)$ versus $\ln(h\nu - E_g)$ by assuming an approximate value of E_g (ii) deducing the value of n based on the slope in this graph. (iii) refining the value of E_g by plotting $(\alpha h\nu)^{1/n}$ versus $h\nu$ and extrapolating the plot to $(\alpha h\nu)^{1/n} = 0$. Figure 9a shows the plot of $\ln(\alpha h\nu)$ versus $\ln(h\nu - E_g)$ for $ZnBiErO_4$. Based on the Figure 9a, the slope of the graph was 1.49048961 and the value of n for $ZnBiErO_4$ was calculated to be 2. Figure 9b shows the plot of $(\alpha h\nu)^{1/2}$ versus $h\nu$ for $ZnBiErO_4$. It was obvious to see that the value of E_g for $ZnBiErO_4$ was calculated to be 1.69 eV, indicating that $ZnBiErO_4$ possessed narrow band gap and the optical transition for $ZnBiErO_4$ was directly allowed.

2.2. Photocatalytic Activity

Figure 10 (cited from [45]) shows the irradiance spectrum of the xenon lamp light. From the diagram, we can learn that the spectrum of xenon lamp is close to the visible light. Therefore, a 500 W xenon lamp was used as a light source with a 400 nm cutoff filter to provide visible light irradiation in this paper. Figure 11 shows temporal spectral changes of aqueous solutions of methyl blue (MB) due to visible light irradiation in the presence of $ZnBiErO_4$. The result illustrated that $ZnBiErO_4$ could photodegrade MB effectively under visible light irradiation and the color of MB solution shallowed gradually when irradiation time increased. Otherwise, it was also obvious to observe that there was a significant reduction in typical MB peaks in 591 nm from the results, demonstrating that the maximum absorption wavelength of MB was 591 nm. The result is close to the study by Cai Jiabia et al., in which the absorbance wavelength of methyl blue is 596 nm [46].

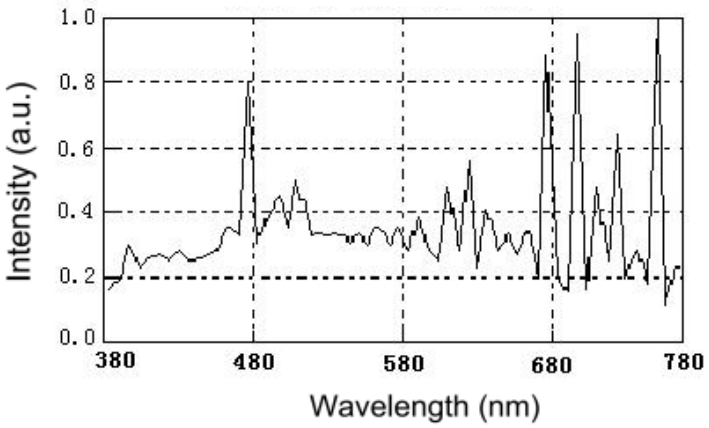

Figure 10. The irradiance spectrum of the Xeon lamp light (cited from [45]).

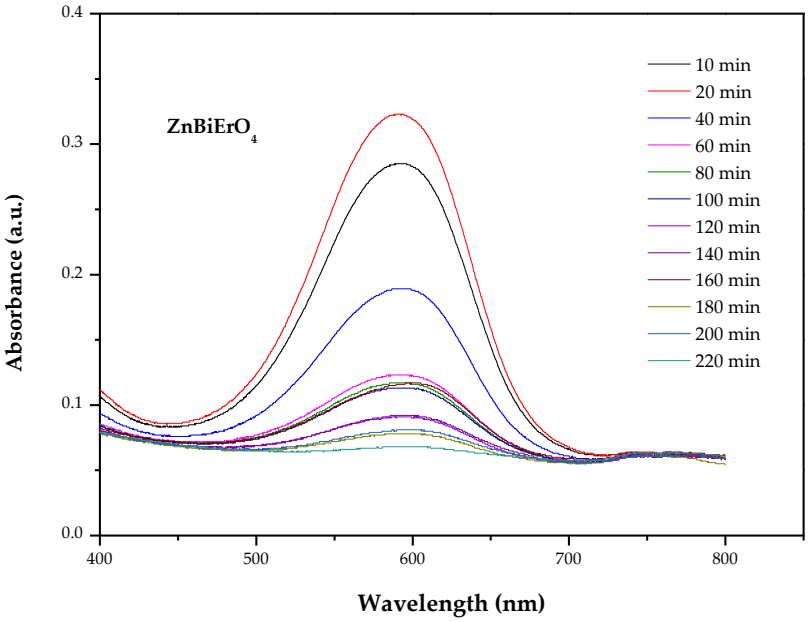

Figure 11. Temporal spectral changes of aqueous solutions of methyl blue due to light irradiation in the presence of $ZnBiErO_4$.

According to the principle of photocatalysis, electron-hole pairs within $ZnBiErO_4$ resulted from the direct absorption of band-gap photons began to diffuse to the surface of $ZnBiErO_4$, as a result, the photocatalytic activity of $ZnBiErO_4$ for degradation of organic compounds might be enhanced. Figure 12 describes the photocatalytic degradation chart of MB under visible light irradiation in the presence of $ZnBiErO_4$, N-doped TiO_2 (N-TiO_2) as well as in the absence of a photocatalyst. Based on the changes in the UV-Vis spectrum of decomposing MB in visible light ($\lambda > 400$ nm) by $ZnBiErO_4$, N-doped TiO_2, it could be seen that both $ZnBiErO_4$ and N-doped TiO_2 could photodegrade MB effectively under visible light irradiation. After visible light irradiation for 220 min, the removal rate of MB was estimated to be 96.99%, 62.39% or 3.31% with $ZnBiErO_4$, N-doped TiO_2 as catalyst, as well as in the absence of a photocatalyst, respectively. From the Figure 12, we can observe that the speed was slower of MB degradation by using $ZnBiErO_4$ or N-doped TiO_2 as a photocatalyst during the later reaction process compared with the speed of 0–60 min. According the results, we supposed that some intermediate products generated during MB degradation occupied active reaction sites on the photocatalytic surface, which could reduce the number of oxygen active radical and the reaction probability between the dye of MB and optical electron-hole pairs [47–49]. The photodegradation rate of MB was about 2.153×10^{-9} mol L^{-1} s^{-1} or 1.385×10^{-9} mol L^{-1} s^{-1} with $ZnBiErO_4$ or N-doped TiO_2 as catalyst under visible light irradiation for 220 min. The self-degradation rate of MB was 0.07348×10^{-9} mol L^{-1} s^{-1} without a catalyst. Furthermore, the photonic efficiency and the quantum yield was estimated to be 0.0452% (λ = 420 nm) and 0.6134% by using $ZnBiErO_4$ as catalyst. Similarly, the photonic efficiency and the quantum yield was estimated to be 0.0291% (λ = 420 nm) and 0.3946% with N-doped TiO_2 as catalyst. It could obviously tell that the photodegradation rate of MB, the photonic efficiency and quantum yield with $ZnBiErO_4$ as catalyst were higher than those with N-doped TiO_2 as catalyst, indicating that the photocatalytic degradation activity of $ZnBiErO_4$ under visible light was higher than N-doped TiO_2. One of the reason might be that a high photonic efficiency and quantum yield could lead to the production of a large number of electron-hole pairs, which were responsible for the photocatalytic degradation reaction directly or indirectly [50]. In addition, the band gap was another factor [51]. The band gap of $ZnBiErO_4$ was calculated to be 1.69 eV and the band gap of N-doped TiO_2 was 2.76 eV, demonstrated that $ZnBiErO_4$ possessed narrower band gap compared with N-doped TiO_2. Therefore, $ZnBiErO_4$ could make use of more irradiation light energy than N-doped

TiO_2, which was more beneficial to generate separate photogenerated electrons and photogenerated holes. Subsequently, the $ZnBiErO_4$ photocatalytic activities were improved. In conclusion, $ZnBiErO_4$ possessed higher photocatalytic activity than N-doped TiO_2.

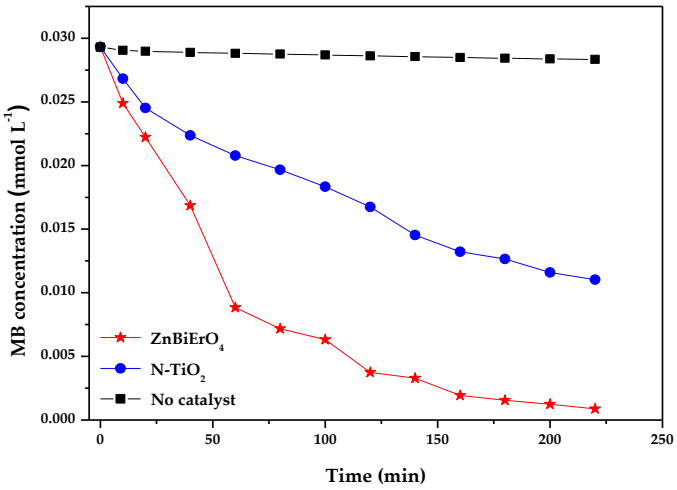

Figure 12. Photocatalytic degradation of methyl blue under visible light irradiation in the presence of $ZnBiErO_4$ and N-TiO_2 as well as in the absence of a photocatalyst.

The changes of total organic carbon (TOC) during photocatalytic degradation of MB in the presence of $ZnBiErO_4$ and N-TiO_2 as well as in the absence of a photocatalyst are shown in Figure 13, which was in accordance with the tendency shown in Figure 12. The measurements of TOC represented the change of organic carbon in MB solution which contained $ZnBiErO_4$ catalyst, N-doped TiO_2 catalyst or no catalyst under visible light irradiation. The gradual decrease of TOC represented the gradual disappearance of organic carbon and the reduce rate of TOC was estimated to be 94.87%, 59.42% or 3.09% after visible light irradiation for 220 min in the presence of $ZnBiErO_4$ and N-TiO_2 as well as in the absence of a photocatalyst. Moreover, the reaction stopped when the light was turned off in this experiment, indicating the obvious light response of $ZnBiErO_4$ photocatalyst. It was illustrated that MB had been converted to other kinds of byproducts and the organic carbon in the MB had not been decomposed to CO_2.

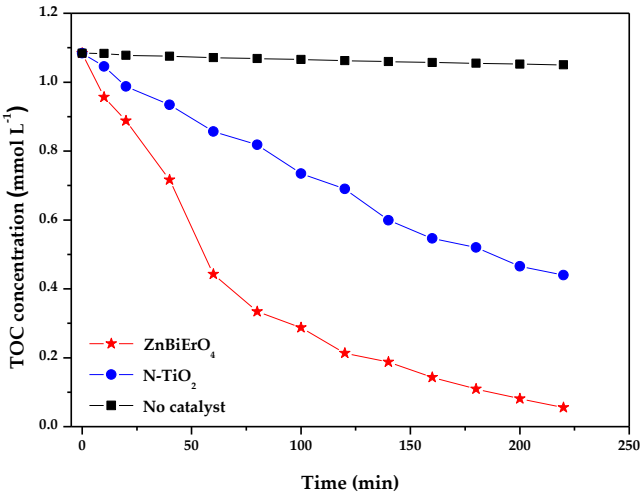

Figure 13. Disappearance of total organic carbon (TOC) during photocatalytic degradation of methyl blue under visible light irradiation in the presence of $ZnBiErO_4$ and N-TiO_2 as well as in the absence of a photocatalyst.

Figure 14 shows the first-order nature of the photocatalytic degradation kinetics with $ZnBiErO_4$ or N-doped TiO_2 as catalyst. A linear correlation between ln (C/C_o) (or ln (TOC/TOC_o)) and the irradiation time could be clearly seen for the photocatalytic degradation of MB by $ZnBiErO_4$ or N-doped TiO_2 under visible light irradiation. According to Figure 14, the first-order rate constant k_C of MB concentration was estimated to be 0.01607 min^{-1} or 0.00435 min^{-1} with $ZnBiErO_4$ or N-doped TiO_2 as catalyst. Based on the result, it was more suitable for $ZnBiErO_4$ to degrade MB under visible light irradiation compared with N-doped TiO_2. Meanwhile, the first-order rate constant K_{TOC} of TOC was estimated to be 0.01313 min^{-1} or 0.00419 min^{-1} with $ZnBiErO_4$ or N-doped TiO_2 as catalyst. The different value between k_C and K_{TOC} illustrated that the photodegradation intermediate products of MB probably appeared during the photocatalytic degradation of MB under visible light irradiation. At the same time, $ZnBiErO_4$ showed a higher mineralization efficiency for MB degradation compared with N-doped TiO_2.

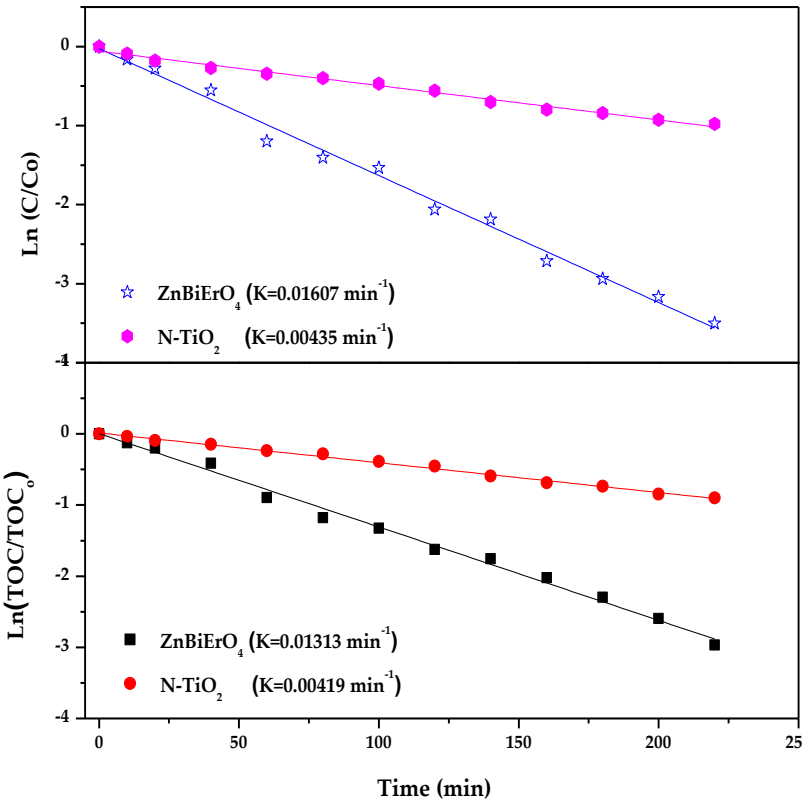

Figure 14. First-order kinetic plots for the photocatalytic degradation of methyl blue with $ZnBiErO_4$ or N-TiO_2 as catalyst under visible light irradiation.

Figure 15 reveals the amount variation of CO_2 which was yielded during the photodegradation of MB with $ZnBiErO_4$ or N-doped TiO_2 as catalyst under visible light irradiation. The amount of CO_2 increased gradually with increasing the irradiation time. After visible light irradiation for 220 min, the CO_2 production of 0.30805 mmol with $ZnBiErO_4$ as catalyst was higher than the CO_2 production of 0.19189 mmol with N-doped TiO_2 as catalyst. It could be distinctly seen from Figures 13 and 15 that the amount of CO_2 production was nearly equal to the amount of removed TOC and the quantity of CO_2 production or the removed TOC was slightly lower than the quantity of reduced MB by using different catalysts. It was demonstrated that MB was mainly mineralized into some inorganic products including CO_2 and H_2O.

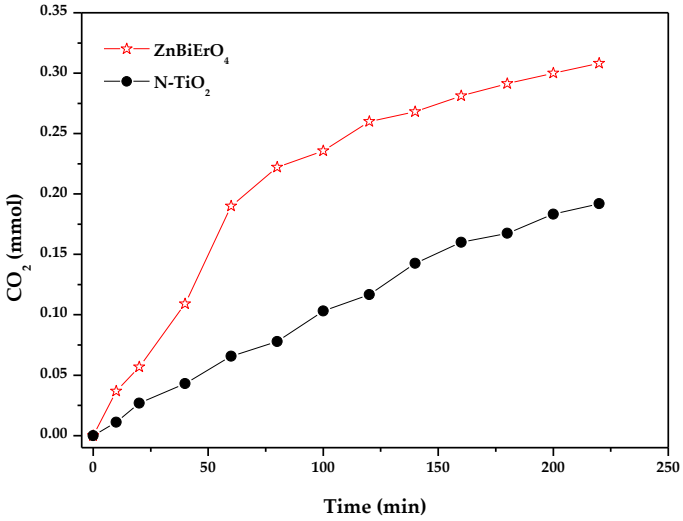

Figure 15. Production of CO_2 during the photocatalytic degradation of methyl blue with $ZnBiErO_4$ or N-TiO_2 as catalyst under visible light irradiation.

The nitrogen and sulfur atoms existed in MB were converted to some inorganic ions such as NO_3^- and SO_4^{2-} as the end products. Figure 16 shows the concentration variation of NO_3^- ions and SO_4^{2-} ions when MB was photodegraded by $ZnBiErO_4$ under visible light irradiation. As the reaction time went by, it could be clearly seen that the concentration of NO_3^- and SO_4^{2-} increased gradually during the photocatalytic degradation of MB with $ZnBiErO_4$ as catalyst. After visible light irradiation for 220 minutes, the concentration of SO_4^{2-} ions was 0.08445 mM with $ZnBiErO_4$ as catalyst, indicating that 93.58% of sulfur from MB was converted into sulfate ions with $ZnBiErO_4$ as catalyst after visible light irradiation for 220 min. Likewise, the concentration of NO_3^- ions was 0.08456 mM with $ZnBiErO_4$ as catalyst during visible light irradiation for 220 min, indicating that 94.46% of nitrogen from MB was converted into nitrate ions with $ZnBiErO_4$ as catalyst after visible light irradiation for 220 min. It was worth noting that the amount of SO_4^{2-} ions released into the solution was lower than the value of stoichiometry. One possible reason might be that part of the sulfur was translated to sulfur-containing volatile compounds such as SO_2. The second possible reason was that some SO_4^{2-} ions were absorbed irreversibly on the surface of the photocatalyst, which had been observed by Lachheb et al. [52]. Regardless of the irreversible absorption of sulfate ions on the surface or not, it was important to stress that the evidence for restrained photocatalytic activity was not noticed. In contrast to the sulfate ions, the amount of nitrate ions at the end of the process was found to follow the expected stoichiometric ratio of three. The molecule of MB was converted to small organic species, which were subsequently mineralized into inorganic products such as SO_4^{2-} ions, NO_3^- ions, CO_2 and H_2O ultimately.

Figure 17 describes the photocatalytic degradation chart of MB under visible light irradiation in the presence of $ZnBiErO_4$, ZnO, Bi_2O_3, Er_2O_3 and mixture which contain ZnO, Bi_2O_3 and Er_2O_3. After visible light irradiation for 220 min, the removal rate of MB was estimated to be 96.99%, 59.35%, 57.44%, 54.30% or 58.53% with $ZnBiErO_4$, ZnO, Bi_2O_3, Er_2O_3 or mixture as catalyst. It could be observed that the photodegradation rate of MB with $ZnBiErO_4$ as catalyst was higher than those with ZnO, Bi_2O_3, Er_2O_3 or mixture as catalyst, indicating that the photocatalytic degradation activity of $ZnBiErO_4$ under visible light was higher than those of ZnO, Bi_2O_3, Er_2O_3 or mixture. By investigating the photocatalytic degradation results of individual oxides and the synergistic effect of its mixture, we could learn that the photocatalytic activities were improved greatly when the new catalyst was formed, proving the justification of using $ZnBiErO_4$ as the photocatalyst.

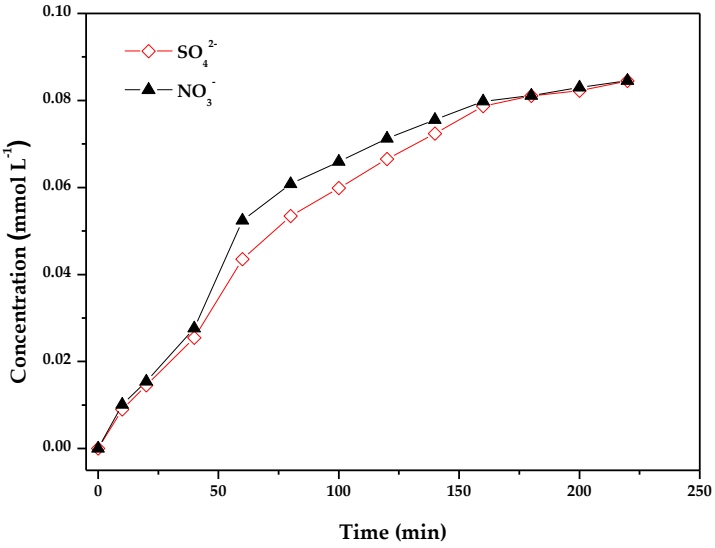

Figure 16. The concentration variation of NO_3^- and SO_4^{2-} during photocatalytic degradation of methyl with $ZnBiErO_4$ as catalyst under visible light irradiation.

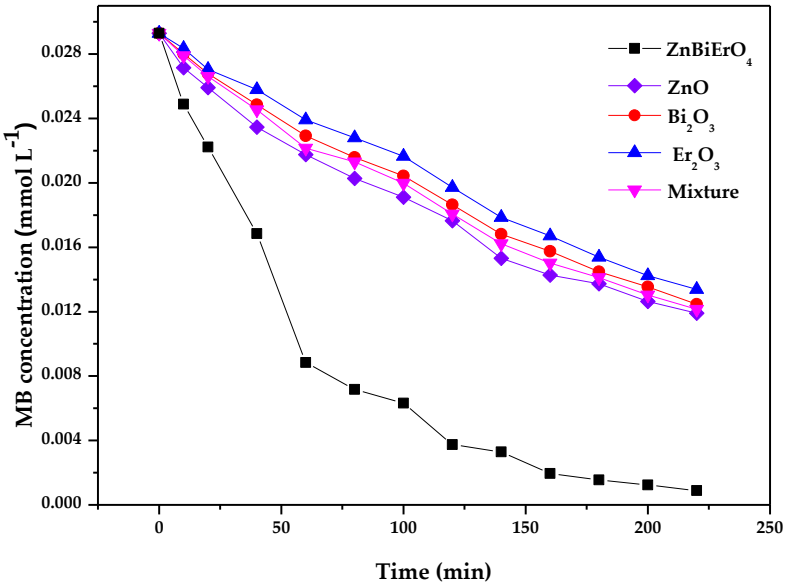

Figure 17. Photocatalytic degradation of methyl blue under visible light irradiation in the presence of $ZnBiErO_4$, ZnO, Bi_2O_3, Er_2O_3 and mixture.

Figures 18 and 19 represent the photocatalytic degradation chart of MB with $ZnBiErO_4$ and commercial P25 as catalyst under visible light irradiation or sunlight irradiation. After visible light irradiation for 220 min, the removal rate of MB was estimated to be 96.99% or 12.01% with $ZnBiErO_4$ or P25 as catalyst. After sunlight irradiation for 220 min, the removal rate of MB was estimated to be 97.85% or 24.51% with $ZnBiErO_4$ or P25 as catalyst. It could be observed that the photodegradation rate of MB with $ZnBiErO_4$ as catalyst was higher than those with P25 as catalyst whether under visible light irradiation or under sunlight irradiation, indicating that the photocatalytic degradation activity of $ZnBiErO_4$ was higher than those of commercial P25.

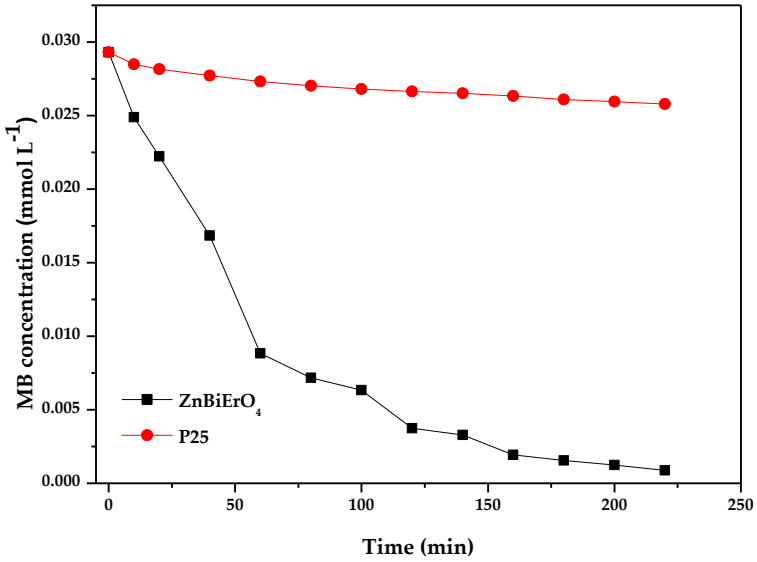

Figure 18. Photocatalytic degradation of methyl blue with $ZnBiErO_4$ or P25 as catalyst under visible light irradiation.

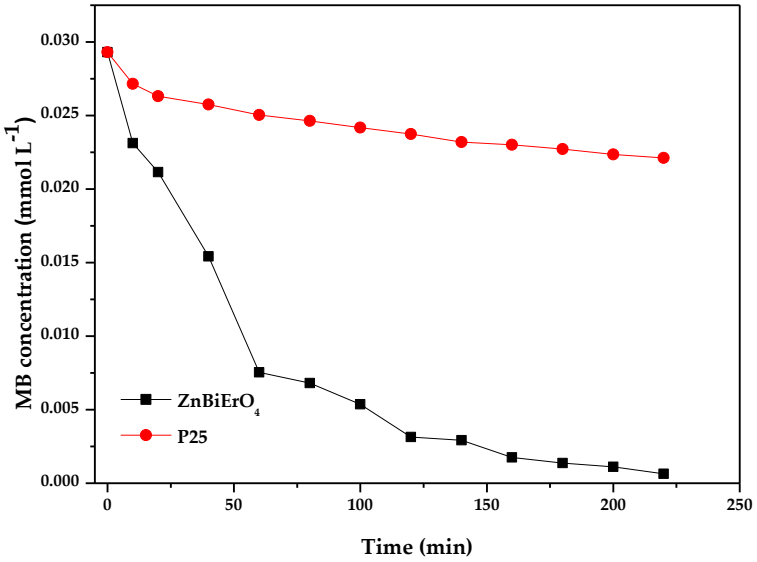

Figure 19. Photocatalytic degradation of methyl blue with $ZnBiErO_4$ or P25 as catalyst under sunlight irradiation.

Figure 20 shows the photocatalytic degradation of phenol with $ZnBiErO_4$ as a photocatalyst under visible light irradiation. According to Figure 20, it was obvious to find that the photocatalytic activity was obtained when colorless phenol was selected as a contaminant model with $ZnBiErO_4$ as photocatalyst. The photocatalytic degradation efficiency of phenol was estimated to be 98.80% when $ZnBiErO_4$ was used as a photocatalyst under visible light irradiation after 220 min, demonstrating that $ZnBiErO_4$ itself had photocatalytic activity and the photosensitive effect was not the main reason in the photodegradation process of MB by using $ZnBiErO_4$ as a photocatalyst [53].

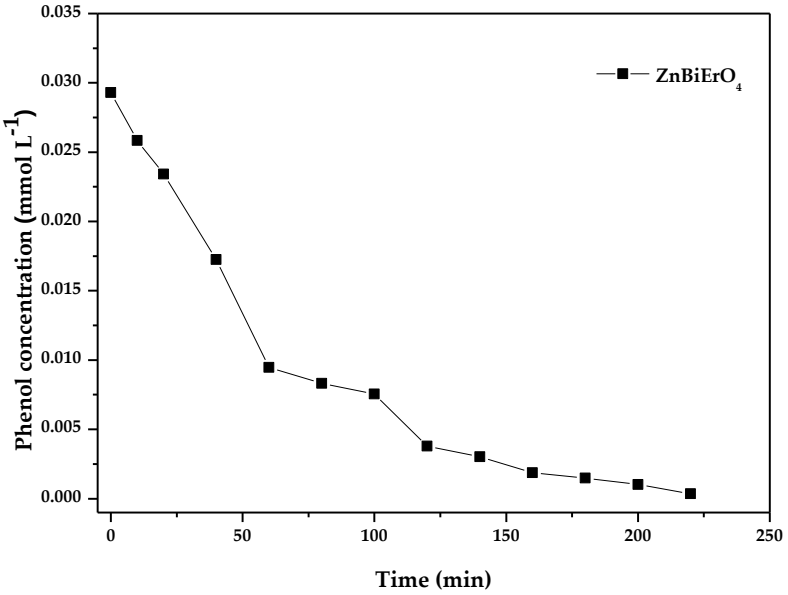

Figure 20. The photocatalytic degradation of phenol with $ZnBiErO_4$ as a photocatalyst under visible light irradiation.

2.3. Photocatalytic Degradation Mechanism

As well as we have known, the organic pollutants can be degraded by the photogenerated reactive species during the photocatalytic reaction, including electrons (e^-), holes (h^+), hydroxyl radicals (•OH) and superoxide radicals ($\bullet O_2^-$). In order to confirm the major reactive species for inducing the degradation of methyl blue with $ZnBiErO_4$ as catalyst under visible light irradiation, radical scavenger experiments were performed by adding various scavengers into the system.

Superoxide dismutase (SOD) with the concentration of 66.7 mg L^{-1}, sodium oxalate with the concentration of 10 mM, H_2O_2 with the concentration of 10 mM and tert-butyl alcohol (TBA) with the concentration of 10 mM were added into the system as scavengers to capture $\bullet O_2^-$, h^+, e^- and •OH, respectively. Figure 21 illustrates photodegradation of methyl blue over $ZnBiErO_4$ in the presence of various scavengers. As shown in Figure 21, after the addition of H_2O_2 as a scavenger for photogenerated electrons (e^-), the photodegradation efficiency of methyl blue remained almost the same compared with the system of no scavenger, demonstrating the minor role of e^- in this process. When tert-butyl alcohol (TBA) was used as the scavenger to capture •OH, the photodegradation activity declined somewhat. However, a significant reduction in the photocatalytic performance was observed in the presence of sodium oxalate and superoxide dismutase (SOD), which captured $\bullet O_2^-$ and h^+ respectively. The results indicate that the photoreaction process in this system is dominated by h^+ and $\bullet O_2^-$. In conclusion, h^+ contribute most to the high activity of the $ZnBiErO_4$ during the degradation of methyl blue. Additionally, $\bullet O_2^-$ radicals have a secondary importance during methyl blue degradation. As for •OH, it may participate in the photodegradation process. However, e^- exhibit almost no activity during methyl blue degradation in the presence of $ZnBiErO_4$.

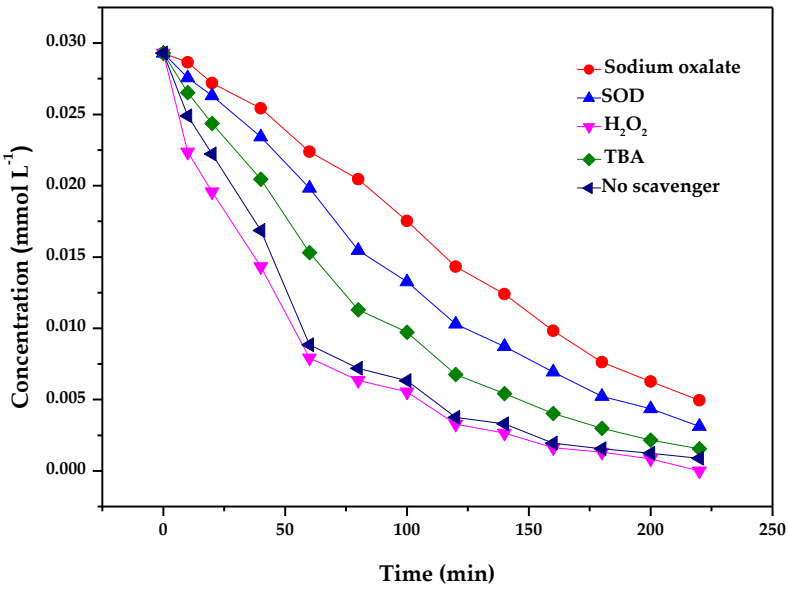

Figure 21. Photodegradation of methyl blue over $ZnBiErO_4$ in the presence of various scavengers: sodium oxalate, superoxide dismutase (SOD), H_2O_2, tert-butyl alcohol (TBA) and no scavenger.

Based on above results, a possible mechanism of photocatalytic activity enhancement could be proposed as the following steps:

Scheme I:

$$ZnBiErO_4 \xrightarrow{\text{Visible light}} h^+ + e^- \quad \text{(R1)}$$

$$e^- + O_2 \rightarrow \cdot O_2^- \quad \text{(R2)}$$

$$h^+ + OH^- \rightarrow \cdot OH \quad \text{(R3)}$$

$$h^+ + \cdot OH + \cdot O_2^- + MB \rightarrow \text{degradation products} \quad \text{(R4)}$$

Scheme II:

$$MB_{(ads)} \xrightarrow{\text{Visible light}} MB^*_{(ads)} \quad \text{(R5)}$$

$$MB^*_{(ads)} + ZnBiErO_4 \rightarrow ZnBiErO_4(e) + MB^+_{(ads)} \quad \text{(R6)}$$

$$ZnBiErO_4(e) + O_2 \rightarrow ZnBiErO_4 + \cdot O_2^- \quad \text{(R7)}$$

$$\cdot O_2^- + MB \rightarrow \text{degradation products} \quad \text{(R8)}$$

Towards scheme I, the electron-hole pairs were generated on the $ZnBiErO_4$ surface upon visible-light excitation (Reaction (R1)), the dissolved oxygen could be activated by the photogenerated electrons to produce superoxide anion radicals (Reaction (R2)), while the holes could react with the absorbed water to form hydroxyl radicals (Reaction (R3)), lastly, the contaminants absorbed on the active sites of $ZnBiErO_4$ was oxidized by the active species (holes, superoxide anion radicals and hydroxyl radicals) (Reaction (R4)). The significant enhancement in photoactivity under visible light irradiation could be ascribed to the reduced recombination of photogenerated electrons and photogenerated holes by $ZnBiErO_4$ [54].

As for the scheme II, MB adsorbed on the surface $ZnBiErO_4$ was excited by visible light irradiation (Reaction (R5)). Subsequently, the electrons were injected from the excited MB to the conduction band of $ZnBiErO_4$ (Reaction (R6)), then, the dissolved oxygen could scavenge the electron to produce superoxide anion radicals (Reaction (R7)), finally, the MB contaminants were degraded by the active species of superoxide anion radicals (Reaction (R8)).

Band gap energy indicated the minimum energy needed to photocatalytically degrade MB. Figure 22 shows the band structure of $ZnBiErO_4$. The positions and width of the conduction band (CB) and the valence band (VB) were obtained after the calculation of the electronic band structure of $ZnBiErO_4$ by the plane-wave-based density functional method. The band structure calculations of $ZnBiErO_4$ were carried out with the program of Cambridge serial total energy package (CASTEP) and first principles simulation. According to above method, we deduced that the band gap energy of $ZnBiErO_4$ was 1.69 eV, at the same time, the valence band of $ZnBiErO_4$ was composed of O 2*p* and Bi 6*s* orbital components and the conduction band of $ZnBiErO_4$ was composed of Zn 4*s* and Er 4*d* orbital components. The results indicated that electron-hole pairs could be produced when $ZnBiErO_4$ absorbed enough photons which were more than needed photons.

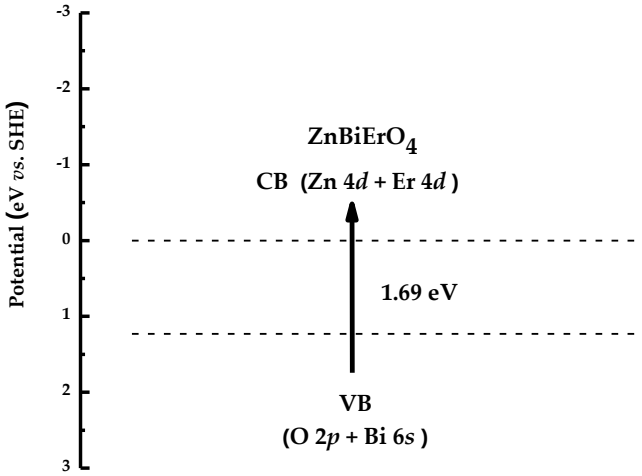

Figure 22. Suggested band structure of $ZnBiErO_4$.

3. Experimental

3.1. Synthesis of $ZnBiErO_4$ and N-Doped TiO_2

The novel $ZnBiErO_4$ photocatalyst was synthesized by a solid-state reaction method. In the first place, ZnO, Bi_2O_3 and Er_2O_3 with purity of 99.99% (Sinopharm Group Chemical Reagent Co., Ltd., Shanghai, China) were mixed with 2:1.1:1 molar ration to serve as raw materials. All chemicals were dried at 200 °C for 4 h before the preparation of the catalyst. Then the precursors were fully mingled with each other, pressed into small columns and put into an alumina crucible (Shenyang Crucible Co., Ltd., Shenyang, China). Finally, calcination was carried out at 1000 °C for 35 h in an electric furnace (KSL 1700X, Hefei Kejing Materials Technology Co., Ltd., Hefei, China). After sintering and grounding within a quartz mortar, ultrafine $ZnBiErO_4$ powder was fabricated. In this study, we prepared about 5 g $ZnBiErO_4$ for characterization and experimental and its costs were about four dollars.

Nitrogen-doped titania (N-doped TiO_2) catalyst was prepared by sol-gel method with tetrabutyl titanate (Shanghai Lingfeng Chemical Reagent Co. Ltd., Shanghai, China) as a precursor and ethanol (Sinopharm Group Chemical Reagent Co., Ltd., Shanghai, China) as solvent. The procedure was as follows: Firstly, 17 mL tetrabutyl titanate and 40 mL absolute ethyl alcohol were combined to serve as to solution A; 40 mL absolute ethyl alcohol, 10 mL glacial acetic acid (Sinopharm Group Chemical Reagent Co., Ltd., Shanghai, China) and 5 mL double distilled water were blended to be solution B; subsequently solution A was added dropwise into solution under vigorous stirring, then a transparent colloidal suspension was formed. Subsequently, aqua ammonia (Shanghai Lingfeng Chemical Reagent Co. Ltd., Shanghai, China), which N/Ti proportion was 8 mol %, was put into the resulting transparent colloidal suspension in the condition of stirring for 1 h. Then the xerogel was generated after being aged for 2 days. The xerogel was grounded into powder which was calcined at

500 °C for 2 h, subsequently above powder was grounded in agate mortar and screened by shaker to obtain N-doped TiO_2 powders.

3.2. Characterization of $ZnBiErO_4$

The crystal structures of $ZnBiErO_4$ was determined by X-ray diffraction (XRD, D/MAX-RB, Rigaku Corporation, Tokyo, Japan) method, which operated at 40 kV and 40 mA with CuKα radiation (λ = 1.54056 Å). The data were collected at 295 K with a step-scan procedure, whose scan range was 2θ = 5–100°. The step interval was 0.02° and the time per step was 1 s. The chemical composition and the surface structure of the compound was determined by means of scanning electron microscope-X-ray energy dispersion spectrum (SEM-EDS, LEO 1530VP, LEO Corporation, Dresden, Germany). Transmission electron microscopy (TEM, Tecnal F20 S-Twin, FEI Corporation, Hillsboro, OR, USA) was used to observe the surface state and structure of the photocatalysts. The particle sizes of the photocatalysts were measured by Malvern's mastersize-2000 particle size analyzer (Malvern Instruments Ltd., Malvern, UK). The content of Zn^{2+}, Bi^{3+}, Er^{3+} and O^{2-} of $ZnBiErO_4$ and the valence state of elements were analyzed by X-ray photoelectron spectroscopy (XPS, ESCALABMK-2, VG Scientific Ltd., London, UK). At the same time, X-ray photoelectron spectroscopy also could be utilized to examine the chemical composition within the depth profile of $ZnBiErO_4$ using the method of argon ion denudation. The photophysical property of $ZnBiErO_4$ was analyzed with an UV-2550 UV-visible spectrophotometer (Shimadzu, UV-2550, Shimadzu Corporation, Kyoto, Japan) in a UV-Vis diffuse reflectance experiment by the dry-pressed disk samples and $BaSO_4$ was used as the reference material.

3.3. Photocatalytic Activity Tests

The photocatalytic activity of $ZnBiErO_4$ was evaluated by photocatalytic degradation of methyl blue ($C_{37}H_{27}N_3O_9S_3$) (Tianjin Bodi Chemical Co., Ltd., Tianjin, China) under visible light. The photoreaction was carried out in a photochemical reaction apparatus (Xujiang Electromechanical Plant, Nanjing, China) with high pressure xenon lamp and Cooling System. The process of our experiments was as follows: 0.3 g photocatalyst powder of N-doped TiO_2 or $ZnBiErO_4$ was added into 300 mL MB aqueous solution in every quartz tube, whose initial concentration was 0.0293 mM and initial pH value was 7.0. In order to ensure the establishment of an adsorption/desorption equilibrium among photocatalysts, the MB dye and atmospheric oxygen, every solution was magnetically stirred in the dark for 45 min. In this paper, a 500 W xenon lamp was used as a light source with a 400 nm cutoff filter to provide visible light irradiation. During visible light illumination, the MB dye pollution was stirred by a magnetic stirrer with 500 rpm and the photocatalyst powder was kept suspended in the solution. One of the quartz tubes was taken out from the photochemical reaction apparatus at various time intervals. Subsequently the suspension was filtered through 0.22 μm membrane filters and the filtrate was analyzed by a Shimadzu UV-2450 UV-Visible spectrometer with the detecting wavelength at 591 nm. Above experiments were performed under oxygen-saturation conditions ($[O_2]$ sat = 1.02×10^{-3} M), pH adjustment was not carried out and the initial pH value was 7.0 and a near constant reaction temperature (20 °C) was maintained by recycling water.

The identification of MB and the intermediate products of MB were measured by liquid chromatograph-mass spectrometer (LC-MS, Thermo Quest LCQ Duo, Thermo Fisher Scientific Corporation, Silicon Valley, CA, USA. Beta Basic-C18 HPLC column: 150 × 2.1 mm, ID of 5 μm, Thermo Fisher Scientific Corporation, Silicon Valley, CA, USA). There were post-photocatalysis solution (20 μL) in the LC-MS system, which were injected automatically. The fluent was composed of 60% methanol and 40% water and the flow rate was 0.2 mL·min^{-1}. MS conditions consisted of an electrospray ionization interface, a capillary temperature of 27 °C with a voltage of 19.00 V, a spray voltage of 5000 V and a constant sheath gas flow rate. The negative ion scan mode and the m/z range swept from 50 to 600 in the spectrum were acquired. The concentration of total organic carbon (TOC) was determined with a TOC analyzer (TOC-5000, Shimadzu Corporation, Kyoto, Japan). Evolution of CO_2 was measured with an intersmat^{TM} IGC120-MB gas chromatograph (Thermo Separation Products

Corporation, Brussels, Belgium). The device equipped with a porapack Q column (3 m in length and with an inner diameter of 0.2 in), which was connected to a catharometer detector. The obtained inorganic products from MB degradation were analyzed by ion chromatograph (DX-300, Dionex Corporation, Sunnyvale, CA, USA). The photonic efficiency was calculated according to the following equation [55,56]:

$$\xi = R/I_0 \quad (2)$$

where ξ is the photonic efficiency (%), R is the rate of MB degradation (Mol L^{-1} s^{-1}) and I_0 is the incident photon flux (Einstein·L^{-1} s^{-1}). The incident photon flux I_0 measured by a radiometer (Model FZ-A, Photoelectric Instrument Factory Beijing Normal University, Beijing, China) was determined to be 4.76×10^{-6} Einstein·L^{-1}·s^{-1} under visible light irradiation.

4. Conclusions

In our study, $ZnBiErO_4$ was prepared by a solid-state reaction method for the first time. The structural properties of $ZnBiErO_4$ was characterized by some material characterization methods and the photocatalytic properties of $ZnBiErO_4$ was also verified in comparison with N-doped TiO_2. XRD results indicated a good agreement between the observed and calculated intensities in a tetragonal crystal structure with space group I41/A. The latticeparameters for $ZnBiErO_4$ were proved to be a = b = 10.255738 Å and c = 9.938888 Å. XPS results confirmed that the synthesized $ZnBiErO_4$ was highly pure under our preparation conditions. The band gap of $ZnBiErO_4$ was estimated to be about 1.69 eV, indicating that $ZnBiErO_4$ could absorb visible light ($\lambda > 400$ nm). Photocatalytic decomposition of aqueous MB was realized under visible light irradiation in the presence of $ZnBiErO_4$ and N-doped TiO_2. The results could obviously tell that the photodegradation rate of MB and the photonic efficiency with $ZnBiErO_4$ as catalyst was higher than those with N-doped TiO_2, which illustrated that $ZnBiErO_4$ exhibited higher photocatalytic activities for MB degradation under visible light irradiation compared with N-doped TiO_2. The photocatalytic degradation of MB with $ZnBiErO_4$ or N-doped TiO_2 as catalyst followed the first-order reaction kinetics. The apparent first-order rate constant of $ZnBiErO_4$ or N-doped TiO_2 was 0.01607 min^{-1} or 0.00435 min^{-1}. The reduction of total organic carbon, formation of inorganic products such as SO_4^{2-} and NO_3^- and the evolution of CO_2 revealed the continuous mineralization of MB during the photocatalytic process. In addition, the possible photocatalytic degradation pathway of MB was deduced under visible light irradiation. Otherwise, the costs (about 0.8 dollars per gram) of $ZnBiErO_4$ photocatalyst are low and the prepared materials are available, proving the availability and feasibility for a large scale application. In conclusion, the results indicated that $ZnBiErO_4$/visible light photocatalysis system might be regarded as a practical method for the treatment of dye wastewater. As this system did not need high pressure of oxygen, heating or any chemical reagents, it has a promising application in purifying and reusing colored aqueous effluents.

Acknowledgments: This work was supported by a grant from China-Israel Joint Research Program in Water Technology and Renewable Energy (No. 5).

Author Contributions: Jingfei Luan was involved with all aspects of the study including conceiving, designing, data interpretation and writing the manuscript. Yan Zhuang performed the experiments and analyzed data. Jingfei Luan and Yan Zhuang wrote the paper. All authors read and approved the manuscript.

Conflicts of Interest: The authors declare no conflict of interest.

References

1. Han, F.; Kambala, V.S.R.; Srinivasan, M.; Rajarathnam, D.; Naidu, R. Tailored titanium dioxide photocatalysts for the degradation of organic dyes in wastewater treatment: A review. *Appl. Catal. A-Gen.* **2009**, *359*, 25–40. [CrossRef]
2. Gupta, V.K.; Suhas. Application of low-cost adsorbents for dye removal—A review. *J. Environ. Manag.* **2009**, *90*, 2313–2342. [CrossRef] [PubMed]

3. Martinez-Huitle, C.A.; Brillas, E. Decontamination of wastewaters containing synthetic organic dyes by electrochemical methods: A general review. *Appl. Catal. B* **2009**, *87*, 105–145. [CrossRef]
4. Nasuha, N.; Hameed, B.H. Adsorption of methylene blue from aqueous solution onto NaOH-modified rejected tea. *Chem. Eng. J.* **2011**, *166*, 783–786. [CrossRef]
5. Safarik, I.; Horska, K.; Safarikova, M. Magnetically modified spent grain for dye removal. *J. Cereal Sci.* **2011**, *53*, 78–80. [CrossRef]
6. Khan, R.; Bhawana, P.; Fulekar, M.H. Microbial decolorization and degradation of synthetic dyes: A review. *Rev. Environ. Sci. Bio/Technol.* **2013**, *12*, 75–97. [CrossRef]
7. Popli, S.; Patel, U.D. Destruction of azo dyes by anaerobic-aerobic sequential biological treatment: A review. *Int. J. Environ. Sci. Technol.* **2015**, *12*, 405–420. [CrossRef]
8. Khanna, A.; Shetty, V.K. Solar photocatalysis for treatment of Acid Yellow-17 (AY-17) dye contaminated water using Ag@TiO_2 core-shell structured nanoparticles. *Environ. Sci. Pollut. Res.* **2013**, *20*, 5692–5707. [CrossRef] [PubMed]
9. Qin, X.; Cheng, H.; Wang, W.; Huang, B.; Zhang, X.; Dai, Y. Three dimensional BiOX (X = Cl, Br and I) hierarchical architectures: Facile ionic liquid-assisted solvothermal synthesis and photocatalysis towards organic dye degradation. *Mater. Lett.* **2013**, *100*, 285–288. [CrossRef]
10. Chang, Y.; Yu, K.; Zhang, C.X.; Li, R.; Zhao, P.Y.; Lou, L.L.; Liu, S.X. Three-dimensionally ordered macroporous WO_3 supported Ag_3PO_4 with enhanced photocatalytic activity and durability. *Appl. Catal. B* **2015**, *176*, 363–373. [CrossRef]
11. Zhu, Y.P.; Li, M.; Liu, Y.L.; Ren, T.Z.; Yuan, Z.Y. Carbon-doped ZnO hybridized homogeneously with graphitic carbon nitride nanocomposites for photocatalysis. *J. Phys. Chem. C* **2014**, *118*, 10963–10971. [CrossRef]
12. Abdullah, H.; Kuo, D.H.; Kuo, Y.R.; Yu, F.A.; Cheng, K.B. Facile synthesis and recyclability of thin nylon film-supported n-type ZnO/p-type Ag_2O nano composite for visible light photocatalytic degradation of organic dye. *J. Phys. Chem. C* **2016**, *120*, 7144–7154. [CrossRef]
13. Teng, F.; Liu, Z.L.; Zhang, A.; Li, M. Photocatalytic performances of Ag_3PO_4 polypods for degradation of dye pollutant under natural indoor weak light irradiation. *Environ. Sci. Technol.* **2015**, *49*, 9489–9494. [CrossRef] [PubMed]
14. Shao, D.L.; Gao, J.; Xin, G.Q.; Wang, Y.P.; Li, L.; Shi, J.; Lian, J.; Koratkar, N.; Sawyer, S. Cl-doped ZnO nanowire arrays on 3D graphene foam with highly efficient field emission and photocatalytic properties. *Small* **2015**, *11*, 4785–4792. [CrossRef] [PubMed]
15. Ao, Y.H.; Wang, K.D.; Wang, P.F.; Wang, C.; Hou, J. Synthesis of novel 2D-2D p-n heterojunction BiOBr/$La_2Ti_2O_7$ composite photocatalyst with enhanced photocatalytic performance under both UV and visible light irradiation. *Appl. Catal. B* **2016**, *194*, 157–168. [CrossRef]
16. Sathyaseelan, B.; Manikandan, E.; Lakshmanan, V.; Baskaran, I.; Sivakumar, K.; Ladchumananandasivam, R.; Kennedy, J.; Maaza, M. Structural, optical and morphological properties of post-growth calcined TiO_2 nanopowder for opto-electronic device application: Ex-situ studies. *J. Alloys Compd.* **2016**, *671*, 486–492. [CrossRef]
17. Yoshinaga, M.; Yamamoto, K.; Sato, N.; Aoki, K.; Morikawa, T.; Muramatsu, A. Remarkably enhanced photocatalytic activity by nickel nanoparticle deposition on sulfur-doped titanium dioxide thin film. *Appl. Catal. B* **2009**, *87*, 239–244. [CrossRef]
18. Erjavec, B.; Hudoklin, P.; Perc, K.; Tisler, T.; Dolenc, M.S.; Pintar, A. Glass fiber-supported TiO_2 photocatalyst: Efficient mineralization and removal of toxicity/estrogenicity of bisphenol A and its analogs. *Appl. Catal. B* **2016**, *183*, 149–158. [CrossRef]
19. Yao, B.H.; Peng, C.; Zhang, W.; Zhang, Q.K.; Niu, J.F.; Zhao, J.E. A novel Fe(III) porphyrin-conjugated TiO_2 visible-light photocatalyst. *Appl. Catal. B* **2015**, *174*, 77–84. [CrossRef]
20. Yaghoubi, H.; Li, Z.; Chen, Y.; Ngo, H.T.; Bhethanabotla, V.R.; Joseph, B.; Ma, S.Q.; Schlaf, R.; Takshi, A. Toward a visible light-driven photocatalyst: The effect of midgap-states-induced energy gap of undoped TiO_2 nanoparticles. *ACS Catal.* **2015**, *5*, 327–335. [CrossRef]
21. Lu, F.; Meng, F. Research evolution of doping modification on TiO_2 photocatalyst. *B. Chin. Ceram. Soc.* **2011**, *30*, 116–119.
22. Park, H.; Park, Y.; Kim, W.; Choi, W. Surface modification of TiO_2 photocatalyst for environmental applications. *J. Photochem. Photobiol. C* **2013**, *15*, 1–20. [CrossRef]

23. Sheng, G.; Li, J.; Wang, S.; Wang, X. Modification to promote visible-light catalytic activity of TiO_2. *Prog. Chem.* **2009**, *21*, 2492–2504.
24. Ding, D.W.; Liu, K.; He, S.N.; Gao, C.B.; Yin, Y.D. Ligand-Exchange Assisted Formation of Au/TiO_2 Schottky Contact for Visible-Light Photocatalysis. *Nano Lett.* **2014**, *14*, 6731–6736. [CrossRef] [PubMed]
25. Pastrana-Martinez, L.M.; Morales-Torres, S.; Figueiredo, J.L.; Faria, J.L.; Silva, A.M.T. Graphene oxide based ultrafiltration membranes for photocatalytic degradation of organic pollutants in salty water. *Water Res.* **2015**, *77*, 179–190. [CrossRef] [PubMed]
26. Rengifo-Herrera, J.A.; Blanco, M.; Wist, J.; Florian, P.; Pizzio, L.R. TiO_2 modified with polyoxotungstates should induce visible-light absorption and high photocatalytic activity through the formation of surface complexes. *Appl. Catal. B* **2016**, *189*, 99–109. [CrossRef]
27. Asahi, R.; Morikawa, T.; Ohwaki, T.; Aoki, K.; Taga, Y. Visible-light photocatalysis in nitrogen-doped titanium oxides. *Science* **2001**, *293*, 269–271. [CrossRef] [PubMed]
28. Mohapatra, P.; Parida, K.M. Photocatalytic activity of sulfate modified titania 3: Decolorization of methylene blue in aqueous solution. *J. Mol. Catal. A-Chem.* **2006**, *258*, 118–123. [CrossRef]
29. Jang, Y.J.; Simer, C.; Ohm, T. Comparison of zinc oxide nanoparticles and its nano-crystalline particles on the photocatalytic degradation of methylene blue. *Mater. Res. Bull.* **2006**, *41*, 67–77. [CrossRef]
30. Li, H.P.; Liu, J.Y.; Hou, W.G.; Du, N.; Zhang, R.J.; Tao, X.T. Synthesis and characterization of $g\text{-}C_3N_4/Bi_2MoO_6$ heterojunctions with enhanced visible light photocatalytic activity. *Appl. Catal. B* **2014**, *160*, 89–97. [CrossRef]
31. Saison, T.; Chemin, N.; Chaneac, C.; Durupthy, O.; Mariey, L.; Mauge, F.; Brezova, V.; Jolivet, J.P. New Insights into $BiVO_4$ Properties as Visible Light Photocatalyst. *J. Phys. Chem. C* **2015**, *119*, 12967–12977. [CrossRef]
32. Ding, X.; Zhao, K.; Zhang, L.Z. Enhanced photocatalytic removal of sodium pentachlorophenate with self-doped Bi_2WO_6 under visible light by generating more superoxide ions. *Environ. Sci. Technol.* **2014**, *48*, 5823–5831. [CrossRef] [PubMed]
33. Yang, S.B.; Xu, D.B.; Chen, B.Y.; Luo, B.F.; Yan, X.; Xiao, L.S.; Shi, W.D. Synthesis and visible-light-driven photocatalytic activity of p-n heterojunction $Ag_2O/NaTaO_3$ nanocubes. *Appl. Surf. Sci.* **2016**, *383*, 214–221. [CrossRef]
34. Wu, L.N.; Fang, S.; Ge, L.; Han, C.C.; Qiu, P.; Xin, Y.J. Facile synthesis of $Ag@CeO_2$ core-shell plasmonic photocatalysts with enhanced visible-light photocatalytic performance. *J. Hazard. Mater.* **2015**, *300*, 93–103. [CrossRef] [PubMed]
35. Christoforidis, K.C.; Montini, T.; Bontempi, E.; Zafeiratos, S.; Jaen, J.J.D.; Fornasiero, P. Synthesis and photocatalytic application of visible-light active $beta\text{-}Fe_2O_3/g\text{-}C_3N_4$ hybrid nanocomposites. *Appl. Catal. B* **2016**, *187*, 171–180. [CrossRef]
36. Cui, B.; Lin, H.; Li, Y.Z.; Li, J.B.; Sun, P.; Zhao, X.C. Photophysical and photocatalytic properties of core-ring struc-tured $NiCo_2O_4$ nanoplatelets. *J. Phys. Chem. C* **2009**, *32*, 14083–14087. [CrossRef]
37. Chen, C.H.; Liang, Y.H.; Zhang, W.D. $ZnFe_2O_4$/MWCNTs composite with enhanced photocatalytic activity under visible-light irradiation. *J. Alloys Compd.* **2010**, *1*, 168–172. [CrossRef]
38. Carta, G.; Casarin, M.; El Habra, N.; Natali, M.; Rossetto, G.; Sada, C.; Tondello, E.; Zanella, P. MOCVD deposition of $CoAl_2O_4$ films. *Electrochim. Acta* **2005**, *50*, 4592–4599. [CrossRef]
39. Tang, J.W.; Zou, Z.G.; Ye, J.H. Efficient photocatalytic decomposition of organic contaminants over $CaBi_2O_4$ under visible-light irradiation. *Angew. Chem.-Int. Ed.* **2004**, *43*, 4463–4466. [CrossRef] [PubMed]
40. Cui, B.; Lin, H.; Zhao, X.C.; Li, J.B.; Li, W.D. Visible light induced photocatalytic activity of $ZnCo_2O_4$ nanoparticles. *Acta Phys.-Chim. Sin.* **2011**, *27*, 2411–2415.
41. Kale, B.B.; Baeg, J.O.; Kong, K.J.; Moon, S.J.; Lee, S.M.; So, W.W. Synthesis and structural analysis of visible light photocatalyst, $ZnBiGaO_4$ for photocatalytic solar hydrogen production. *Int. J. Energy Res.* **2010**, *34*, 404–411. [CrossRef]
42. Arshadnia, I.; Movahedi, M.; Rasouli, N. $MgFe_2O_4$ and $MgFe_2O_4/ZnFe_2O_4$ coated with polyaniline as a magnetically separable photocatalyst for removal of a two dye mixture in aqueous solution. *Res. Chem. Intermed.* **2017**, *43*, 4459–4474. [CrossRef]
43. Tang, J.W.; Zou, Z.G.; Yin, J.; Ye, J. Photocatalytic degradation of methylene blue on Caln(2)O(4) under visible light irradiation. *Chem. Phys. Lett.* **2003**, *382*, 175–179. [CrossRef]
44. Tauc, J.; Grigorov, R.; Vancu, A. Optical properties and electronic structure of amorphous germanium. *Phys. Status Solidi* **1966**, *15*, 627–637. [CrossRef]

45. Xujiang Electromechanical Plant, Nanjing, China. Available online: http://www.njxu.com (accessed on 12 February 2018).
46. Cai, J.B.; Wu, X.Q.; Li, Y.H.; Lin, Y.; Yang, H.; Li, S.X. Noble metal sandwich-like TiO_2@Pt@C_3N_4 hollow spheres enhance photocatalytic performance. *J. Colloid Interface Sci.* **2018**, *514*, 791–800. [CrossRef] [PubMed]
47. Vaiano, V.; Sacco, O.; Sannino, D.; Ciambelli, P. Nanostructured N-doped TiO_2 coated on glass spheres for the photocatalytic removal of organic dyes under UV or visible light irradiation. *Appl. Catal. B* **2015**, *170*, 153–161. [CrossRef]
48. Klein, M.; Nadolna, J.; Golabiewska, A.; Mazierski, P.; Klimczuk, T.; Remita, H.; Zaleska-Medynska, A. The effect of metal cluster deposition route on structure and photocatalytic activity of mono- and bimetallic nanoparticles supported on TiO_2 by radiolytic method. *Appl. Surf. Sci.* **2016**, *378*, 37–48. [CrossRef]
49. Jantawasu, P.; Sreethawong, T.; Chavadej, S. Photocatalytic activity of nanocrystalline mesoporous-assembled TiO_2 photocatalyst for degradation of methyl orange monoazo dye in aqueous wastewater. *Chem. Eng. J.* **2009**, *155*, 223–233. [CrossRef]
50. Guesh, K.; Marquez-Alvarez, C.; Chebude, Y.; Diaz, I. Enhanced photocatalytic activity of supported TiO_2 by selective surface modification of zeolite Y. *Appl. Surf. Sci.* **2016**, *378*, 473–478. [CrossRef]
51. Abdelhaleem, A.; Chu, W. Photodegradation of 4-chlorophenoxyacetic acid under visible LED activated N-doped TiO_2 and the mechanism of stepwise rate increment of the reused catalyst. *J. Hazard. Mater.* **2017**, *338*, 491–501. [CrossRef] [PubMed]
52. Lachheb, H.; Puzenat, E.; Houas, A.; Ksibi, M.; Elaloui, E.; Guillard, C.; Herrmann, J.M. Photocatalytic degradation of various types of dyes (Alizarin S, Crocein Orange G, Methyl Red, Congo Red, Methylene Blue) in water by UV-irradiated titania. *Appl. Catal. B* **2002**, *39*, 75–90. [CrossRef]
53. Calza, P.; Rigo, L.; Sangermano, M. Investigations of photocatalytic activities of photosensitive semiconductors dispersed into epoxy matrix. *Appl. Catal. B Environ.* **2011**, *106*, 657–663. [CrossRef]
54. Nasr, C.; Vinodgopal, K.; Fisher, L.; Hotchandani, S.; Chattopadhyay, A.K.; Kamat, P.V. Environmental photochemistry on semiconductor surfaces. Visible light induced degradation of a textile diazo dye, naphthol blue black, on TiO_2 nanoparticles. *J. Phys. Chem.* **1996**, *100*, 8436–8442. [CrossRef]
55. Marugan, J.; Hufschmidt, D.; Sagawe, G.; Selzer, V.; Bahnemann, D. Optical density and photonic efficiency of silica-supported TiO_2 photocatalysts. *Water Res.* **2006**, *40*, 833–839. [CrossRef] [PubMed]
56. Sakthivel, S.; Shankar, M.V.; Palanichamy, M.; Arabindoo, B.; Bahnemann, D.W.; Murugesan, V. Enhancement of photocatalytic activity by metal deposition: Characterisation and photonic efficiency of Pt, Au and Pd deposited on TiO_2 catalyst. *Water Res.* **2004**, *38*, 3001–3008. [CrossRef] [PubMed]